Stress Concentration at Circular Cutouts in Buffer Strip Laminates

E. S. Meyer*
McDonnell Aircraft Company, McDonnell Douglas Corporation, St. Louis, Missouri 63166
and
L. R. Dharani†
University of Missouri—Rolla, Rolla, Missouri 65401

Composite laminates containing notches such as cracks and cutouts suffer a substantial reduction in static strength due to high stress concentrations. One of the methods for reducing such stress concentration has been to use a hybrid (buffer strip) construction. In the present study an approximate analytical model is developed for determining the stresses, strains, and stress concentration in a buffer strip laminate containing a circular cutout. The method is based on the classical shear-lag stress-displacement relations. An extensive parametric study is presented, using a number of material combinations, to understand the effect of stiffness and strength of the buffer strips on the laminate notched strength. The results show that lower modulus and higher failure strain buffer strips are most efficient in increasing the notched strength of laminates with circular cutouts.

I. Introduction

COMPOSITE laminates containing notches such as cracks and cutouts suffer a substantial reduction in static strength due to high stress concentrations. A number of methods to reduce such stress concentrations have been considered. One such method that evolved from the stringer reinforced metallic construction is the buffer strip or hybrid laminate.[1-5] A buffer strip laminate is built by replacing specific fibers of a laminate, usually zero-degree fibers, with fibers of different moduli. A typical buffer strip laminate is shown in Fig. 1. The buffer strips are usually narrow and relatively far apart such that they do not affect the stiffness, weight, or the unnotched strength of the laminate, but result in substantial reduction in stress concentration at discontinuities.[1-5]

Analytical models have been developed for determining the stresses, displacements, and stress concentration factors in buffer strip laminates containing cracks[6,7] and rectangular cutouts.[8] These models assume the laminate to be unidirectional with the notch being normal to the fibers and the loading direction. Further, the fibers are assumed to carry all the axial load, while the matrix transfers load between fibers by shear stresses only. This assumption leads to the use of shear-lag displacement relations[9-11] by virtue of which the axial equilibrium equations become independent of transverse displacement. To obtain the fiber axial stresses and the matrix shear stresses, only the axial equilibrium equation needs to be considered.[11]

The intent of the present study is to develop an approximate analytical model for determining the stresses, strains, and stress concentration in a buffer strip laminate containing a circular cutout. Jones[12,13] presented a shear lag solution to the problem of a circular cutout in a unidirectional infinite plane subjected to a uniform axial stress. In this article we modify the above solution for a finite width unidirectional region and then employ the procedure developed for the buffer strip laminate with damage[6] to obtain the solution for the circular cutout in a buffer strip laminate. The idealized geometry considered in the analysis is shown in Fig. 2. The simplified model consists of three unidirectional regions of different properties. The two buffer strips (region 2) are located on either side of the main panel (region 1), while region 3, consisting of two half-planes, represents the remainder of the laminate that is not significantly affected by the presence of the cutout. This idealized geometry differs from the real construction in that it has two buffer strips and two half-planes symmetrically placed with respect to the main panel, rather than a periodic array of buffer strips and main panels. The stresses around the cutout are predominantly affected by the buffer strip in the immediate neighborhood of the cutout. The effect of buffer strips farther away from the cutout influences the stresses to a lesser degree, which would be, to some extent, proportional to the composite laminate modulus in a rule-of-mixture sense. Since, in general, the buffer strips constitute a small percent of the total volume of the laminate, the laminate modulus is very close to that of the main panel. Based on these two factors, therefore, the idealization of periodic buffer strips by a pair of half-planes having the same modulus as the main panel should give a geometry that is mathematically tractable yet represents the behavior of an actual unidirectional buffer strip laminate. In the model, regions 1 and 2 are finite width strips, the solution of which can be obtained from that of a half-plane as a special case.[6] Therefore, the basic solution needed in the analysis of the idealized buffer strip problem is that of a unidirectional half-plane with damage, and this will be developed first. Then, the complete solution for the buffer strip laminate will be developed by matching the shear stresses at the interfaces. Some typical results are then presented.

II. Unidirectional Half-Plane with a Circular Cutout

A unidirectional array of parallel fibers with a longitudinal split in the matrix and an arbitrary number of broken fibers in the form of a circular cutout is shown in Fig. 3. The laminate is subjected to prescribed shear stresses $\tau_a(y)$ along the free edge and $\tau_b(y)$ along the split, and a remote uniform tensile stress in the axial direction. Since the loading is symmetric, only the upper half of the laminate is considered in this analysis.

The fibers are taken to be of much higher strength and extensional stiffness than the matrix and all of the axial load

Received March 5, 1991; revision received May 16, 1991; accepted for publication May 26, 1991.

*Lead Engineer, Strength Department.
†Associate Professor, Department of Mechanical and Aerospace Engineering and Engineering Mechanics.

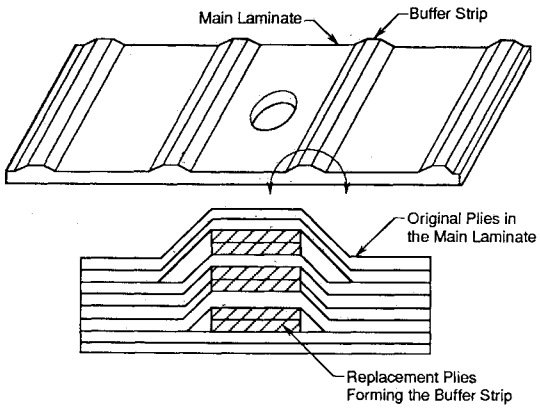

Fig. 1 Typical buffer strip laminate.

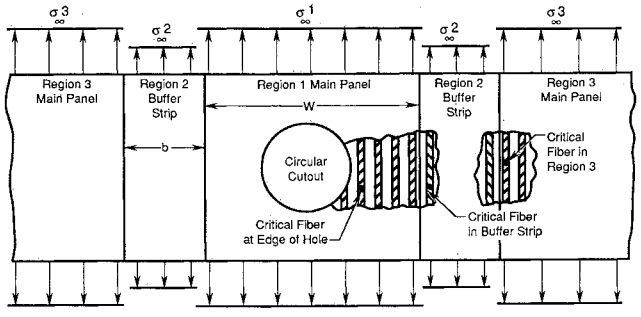

Fig. 2 Buffer strip laminate geometry.

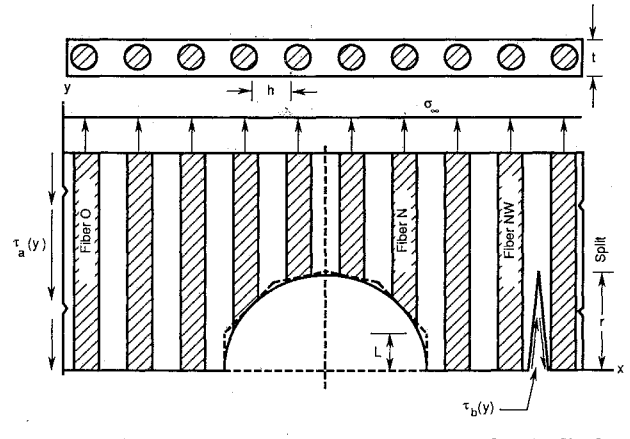

Fig. 3 Laminate geometry with circular cutout and longitudinal matrix splitting.

is assumed to be carried by the fibers with the matrix transferring load by shear stresses as given by the classical shear-lag assumption.[9-11] The axial fiber stress, $\sigma_n(y)$, and the matrix shear stress, $\tau_n(y)$, are then given by the simple relations

$$\sigma_n(y) = E_F \frac{dv_n(y)}{dy} \tag{1}$$

$$\tau_n(y) = \frac{G_M}{h}[v_n(y) - v_{n-1}(y)] \tag{2}$$

where $v_n(y)$ is the displacement of fiber n, E_F is the Young's modulus of the fiber, G_M is shear modulus of the matrix, and h is the shear transfer distance.

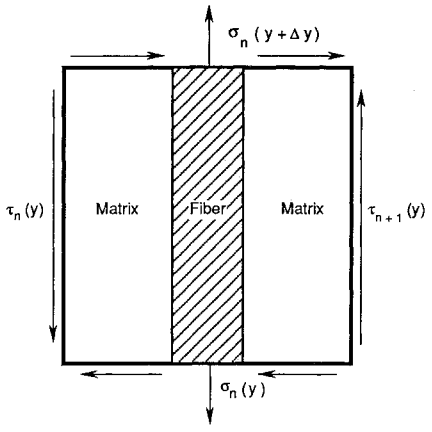

Fig. 4 Free body diagram of typical element, n.

By virtue of the shear-lag assumption, the longitudinal and transverse equilibrium equations become decoupled and the fiber axial displacements and stresses can be obtained without solving the transverse equilibrium equation. Therefore, only the equilibrium equation in the longitudinal (axial) direction will be considered. With reference to the free-body diagram of a typical fiber-matrix region shown in Fig. 4, the equilibrium equation in the longitudinal direction, for all elements of the regions shown in Fig. 3, is given by

$$\frac{A_F}{t}\frac{d\sigma_n(y)}{dy} + \tau_{n+1}(y) - \tau_n(y) = \delta_{no}$$
$$[\tau_a(y) - \tau_n(y)]\{\delta_{nP} - \delta_{n(N+1)}\}\langle y - L\rangle\tau_n(y)$$
$$+ \langle y - r\rangle\{\delta_{nNW}[\tau_{n+1}(y) - \tau_b(y)] + \delta_{n(NW+1)}$$
$$[\tau_b(y) - \tau_n(y)]\} \tag{3}$$

where $\langle y - L\rangle$ is a step function such that $\langle y - L\rangle = 1$ for $y \le L$ and $\langle y - L\rangle = 0$ for $y > L$, and δ_{mn} is Kronecker symbol with $\delta_{mn} = 0$ for $m \neq n$ and $\delta_{mn} = 1$ for $m = n$. Using the shear-lag stress-displacement relations, Eqs. (1) and (2) in the above equilibrium equations, a set of differential-difference equations in terms of displacements, v_n, is first obtained. Then, the following changes in the variables are made:

$$y = \psi\eta \qquad \text{and} \qquad v_n = \phi V_n$$

where

$$\psi = \left[\frac{A_F E_F h}{G_M t}\right]^{1/2} \qquad \phi = \left[\frac{A_F h}{E_F G_M t}\right]^{1/2} \sigma_\infty$$

so that

$$\sigma_n = E_F \frac{dv_n}{dy} = \sigma_\infty \bar{\sigma}_n$$

$$\tau_n = \chi(v_n - v_{n-1}) = \chi\bar{\tau}_n$$

$$r = \psi\beta, \qquad L = \psi\gamma$$

$$\chi = \frac{G_M}{h}\phi \tag{4}$$

with η, β, $\bar{\sigma}_n$, $\bar{\tau}_n$, and $V_n(\eta)$ being nondimensional.

The resulting equilibrium equation in nondimensional form is then given by

$$\frac{d^2Vn}{d\eta 2} + V_{n+1} - 2V_n + V_{n-1} = \delta_{no}[V_{n+1} - V_n + \bar{\tau}_a]$$
$$\{\delta_{nP} - \delta_{n(N+1)}\}[V_n + V_{n-1}]\langle \eta - \gamma \rangle$$
$$+ \langle \eta - \beta \rangle \{\delta_{n(NW)}[V_{n+1} - V_n - \bar{\tau}_b]$$
$$+ \delta_{n(NW+1)}[\bar{\tau}_b + V_n - V_{n-1}]\} \quad (5)$$

where $\bar{\tau}_a(\eta) = \tau_a(y)/\chi$; $\bar{\tau}_b(\eta) = \tau_b(y)/\chi$; $g_N(\eta) = V_{N+1} - V_N$; and $g_{NW}(\eta) = V_{NW+1} - V_{NW}$.

By making use of the even-valued Fourier transforms and the orthogonality property of the circular functions, the above differential-difference equations can be written in the form of a single differential equation[11] valid for all values of η and n.

To develop the stress-free boundary conditions on the hole surface, first consider an unnotched laminate having uniform applied stress at infinity and determine the fiber stresses on a circular region having the radius of the desired cutout. The negative of these stresses are then the appropriate boundary stresses to be applied to the edge of the circular hole in a laminate having vanishing stresses and displacements at infinity. The superposition of the above two solutions is depicted in Fig. 5. Unlike the element shown in Fig. 4, a typical element at the boundary of the circular hole is triangular in shape. A series of these inclined elements are joined together to form an approximation of the circular boundary.[13] For each element a small vertical boundary exists on which the shear stress, as given by the shear-lag assumption, will not be zero. The largest such surface is between the last broken and first unbroken fiber, indicated by L in Fig. 3. The stress-free boundary condition in this vertical segment L is satisified. Due to shear-lag assumptions it is only necessary to solve the axial equilibrium equation in order to obtain the axial stresses and displacements. Therefore, boundary condition in the axial (fiber) direction along the cutout edge is the only one needed and is given later in this section.

The appropriate boundary condition for vanishing stresses and displacements at infinity is

$$V_n(\eta) = 0, \frac{dV_n(\eta)}{d\eta} = 0, \text{ as } \eta \to \infty \text{ for all fibers} \quad (6)$$

For all unbroken fibers an additional boundary condition is

$$V_n(\eta) = 0 \quad \text{at} \quad \eta = 0 \quad (7)$$

The solution to Eq. (5) satisfying the above boundary conditions is given by

$$V_n(\eta) = \frac{2}{\pi}\int_0^\pi e^{-\delta\eta} \sum_{m=0}^{M} B_m c(m)c(n)\, d\theta$$
$$- \frac{1}{\pi}\int_0^\pi \frac{1}{\delta}\cos(\theta/2) \int_0^\infty D(\delta, \eta, t)\bar{\tau}_a(t)\, dtc(n)\, d\theta$$
$$- \frac{1}{\pi}\int_0^\pi \frac{F_{NW}}{\delta} \int_0^\beta D(\delta, \eta, t)[g_{NW}(t) - \bar{\tau}_b(t)]\, dtc(n)\, d\theta$$
$$- \frac{1}{\pi}\int_0^\pi \frac{F_N}{\delta} \int_0^\gamma D(\delta, \eta, t) g_N(t)\, dtc(n)\, d\theta \quad (8)$$

where $\delta^2 = 4\sin^2(\theta/2)$; $c(n) = \cos[(n + 1/2)\theta]$; $F_{NW} = \cos[(NW + 1/2)\theta] - \cos[(NW + 3/2)\theta]$; $F_N = -\cos[(N + 3/2)\theta]$; and $D(\delta,\eta,t) = e^{-\delta|\eta - t|} - e^{-\delta(\eta + t)}$.

The unknown Fourier constants B_m may be solved for by implementation of the appropriate boundary condition at the circular cutout. Following Jones,[12,13] the boundary conditions for the circular cutout problem can be derived as

$$\frac{dV_n}{d\eta} + \frac{\alpha_n}{[1 - \alpha_n^2]^{1/2} H_0}(V_{n+1} - V_n) = -1 \quad (9)$$

where

$$\alpha_n = \frac{2n + 1}{2N + 2}$$

$$H_0 = \left[\frac{A_F E_F}{G_M h t}\right]^{1/2}$$

The above boundary condition must be satisfied at the appropriate η value along the boundary of the hole. The correct value for this evaluation will be the midpoint of the fiber in question, the axial coordinate of which can be written as

$$\eta(n) = \eta_n = \frac{N + 1}{H_0}[1 - \alpha_n^2]^{1/2} \quad (10)$$

and the normalized split length, γ, is set equal to the appropriate length as given by

$$\gamma = \frac{1}{2H_0[1 - \alpha_n^2]^{1/2}} \quad (11)$$

The boundary condition for the circular hole problem now reduces to a set of linear algebraic equations.

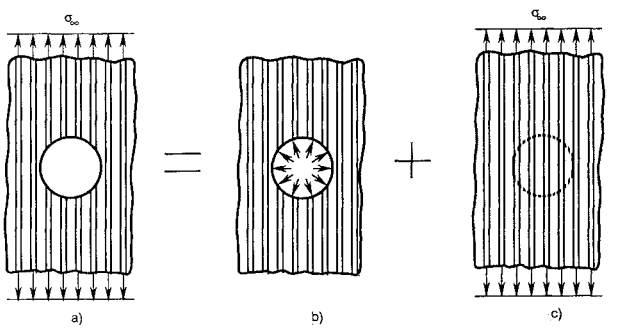

Fig. 5 Superposition of circular cutout problem.

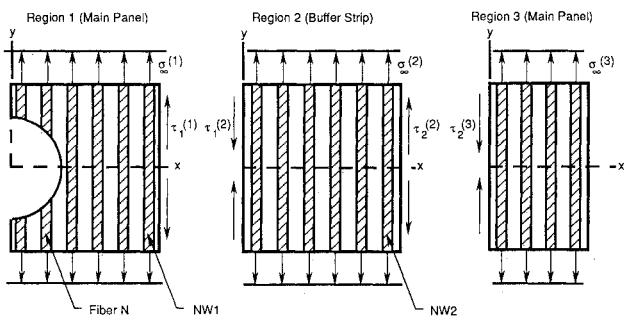

Fig. 6 Solution to symmetric buffer strip laminate.

III. Symmetric Buffer Strip Laminates

Since the laminate shown in Fig. 2 is symmetric about the x- and y-axes only the upper right quadrant need be considered in the analysis. Figure 6 shows the three distinct regions of the laminate. Region 1 is a finite width unidirectional strip with a circular cutout modeled with broken fibers and sub-

jected to remote tensile stress $\sigma_\infty^{(1)}$ and varying shear stresses, $\tau_1^{(1)}(y)$, along the vertical edges. The solution of this region can be obtained by setting the split length (β) equal to infinity in the basic solution obtained in the previous section. Region 2 is a unidirectional finite width strip subjected to a uniform remote tensile stress $\sigma_\infty^{(2)}$ and varying shear stresses $\tau_1^{(2)}(y)$ and $\tau_2^{(2)}(y)$, along the vertical edges and the solution for this is also obtained by setting the split length equal to infinity in the basic solution. Region 3 is a unidirectional half-plane subjected to a uniform remote tensile stress $\sigma_\infty^{(3)}$ and varying shear stress $\tau_2^{(3)}(y)$ along the vertical edge, and the solution is obtained by setting the split length equal to zero in the basic solution. Thus the solutions for the three regions are known for given applied shear and axial stresses.

The spatial variables, stresses, and displacements are normalized as in the previous section using superscripts 1, 2, and 3 to designate quantities corresponding to regions 1, 2, and 3, respectively. The relationships between the actual and normalized quantities are given as follows:

$$\psi^{(1)}\eta = \psi^{(2)}\zeta = \psi^{(3)}\xi = y$$

$$\bar{\tau}_j^{(i)} = \tau_j^{(i)}/x$$

$$v_n^{(i)} = \phi^{(i)}V_n^{(i)} \qquad i = 1, 2, 3 \text{ and } j = 1, 2 \tag{12}$$

Since the remote strains are equal in the three regions, the remote stresses are proportional to Young's moduli.

When the three regions of Fig. 6 are assembled together, the shear stress at the interfaces are unknown but from continuity the shear stresses on each of the adjacent regions must be equal at their respective interfaces. Further, as the shear stress is directly related to the distortion of the matrix from the shear-lag assumption, it follows that these stresses must be proportional to the differences in the displacement of the adjoining fibers of the adjacent regions.[6] These conditions result in the following equations:

$$\tau_j^{(i)}(y) = \tau_j^{(i+1)}(y) \tag{13}$$

$$\tau_j^{(i)}(y) = (G_M/h)_j[v_o^{(i+1)}(y) - v_{NWj}^{(i)}(y)] \tag{14}$$

where $(G_M/h)_j$ is the shear stiffness of the interface j. As before, functions $g_{NW}^{(1)}(\eta)$ and $g_{NW}^{(2)}(\xi)$ are defined for the finite width regions 1 and 2, respectively.

The complete solution to the symmetric buffer strip laminate is obtained by satisfying the matching condition at the interfaces, Eqs. (13) and (14), and the stress boundary conditions on the edges of the hole (broken fibers). The solution of this problem reduces to a series equation coupled with five integral equations involving the unknown Fourier constants, B_m, corresponding to the broken fibers modeling the circular cutout in region 1 and the unknown interfacial shear stresses $\tau_i^{-(1)}(\eta)$ and $\tau_2^{-(2)}(\xi)$, and the two functions $g_{NW}^{(1)}(\eta)$, $g_{NW}^{(2)}(\xi)$ representing the finite width of the regions 1 and 2, and $g_N^{(1)}(\eta)$, representing the mismatch of the last inclined element with the x-axis as shown in Fig. 3. The governing equations can be written in the following form:

$$\sum_{m=0}^{M} B_m K_{11}(m,n,\eta_n) + \sum_{j=2}^{6} \int_0^{\gamma_j} K_{ij}(n,\eta_n,t) f_j(t)\, dt = 1$$

$$\text{for fibers } n = 0, \ldots, N$$

$$\sum_{m=0}^{M} B_m K_{i1}(m,\zeta) + f_i(\xi) + \sum_{j=2}^{6} \int_0^{\gamma_j} K_{ij}(\zeta,t) f_j(t)\, dt = 0$$

$$\text{for } i = 2, \ldots, 6 \tag{15}$$

where $\gamma_2 = \gamma_3 = \gamma_5 = \gamma_6 = \infty$, $\gamma_4 = \gamma$, functions f_i stand for $\bar{\tau}_1^{(1)}(\eta)$, $g_N^{(1)}(\eta)$, $\bar{\tau}_2^{(2)}(\xi)$, and $g_{NW}^{(2)}(\xi)$, respectively, $\zeta = \eta$ for region 1 and $\zeta = \xi$ for region 2, and functions K_{ij} are defined in the appendix.

The above six integral equations contain the unknown Fourier constants B_m and the unknown functions f_i. The solution is developed by representing the integrals over a semi-infinite interval using a Gauss-Laguerre quadrature formula and the integrals over a finite interval using a Gauss-Legendre quadrature formula. These equations then reduce to a system of linear algebraic equations having as unknowns the Fourier constants and the values of the unknown functions at quadrature points.

IV. Results and Discussion

Some typical results are presented in this section for a buffer strip laminate containing a circular cutout. The particular geometry consists of a cutout that covers the entire width of the main panel, region 1 in Fig. 2, so that it is bridging the buffer strips; for this case the diameter of the cutout is equal to the width of the central main panel, w. The width of the buffer strip $b = w/3$. The critical fibers for this configuration are, then, the first fiber in the buffer strip (first unbroken fiber at the cutout edge) and the first fiber in region 3, critical fiber in the main panel. The stress concentrations in the buffer strip (K_{TBS}) and in the main panel (K_{TMP}) are defined with reference to Fig. 2 as

$$K_{TBS} = \sigma_0^{(2)}/\sigma_\infty^{(1)}$$

$$K_{TMP} = \sigma_0^{(3)}/\sigma_\infty^{(1)} \tag{16}$$

where $\sigma_0^{(2)}$ is the stress in the first fiber of the buffer strip and $\sigma_0^{(3)}$ is the stress in the first fiber of the main panel (region 3), and $\sigma_\infty^{(1)}$ is the remote applied stress in the main panel.

A number of fiber materials are chosen for parametric study where both the main panel and the buffer strips are changed. For this purpose the stiffness ratio (R_1) and the strength ratio (S_1) are defined as

$$R_1 = \sqrt{\frac{E_F^{(2)}}{E_F^{(1)}}}$$

$$S_1 = \frac{\sigma_{ult}^{(2)}}{\sigma_{ult}^{(1)}} \tag{17}$$

where $E_F^{(2)}$ and $\sigma_{ult}^{(2)}$ are the Young's modulus and ultimate strength of the buffer strip material and $E_F^{(1)}$ and $\sigma_{ult}^{(1)}$ are the corresponding properties of the main panel (regions 1 and 3). The materials shown in Table 1 are chosen so as to cover among others the following characteristics for the buffer strips: stiffer and stronger ($R_1 > 1$, $S_1 > 1$), stiffer and weaker ($R_1 > 1$, $S_1 < 1$), softer and stronger ($R_1 < 1$, $S_1 > 1$), softer and weaker ($R_1 < 1$, $S_1 < 1$), equally stiff but stronger or weaker ($R_1 = 1$, $S_1 > 1$ or $S_1 < 1$). Stress concentration calculations do not involve the ultimate strengths or the strength ratio, S_1.

Table 1 Material properties (fiber)

Material ID#	Material description	Modulus Msi(GPa)	Tensile strength ksi(Mpa)
1	PIBG, P-140	140 (965)	250 (1725)
2	PIBG, P-100	100 (690)	250 (1725)
3	PABG, ultrahigh modulus	75 (520)	150 (1035)
4	PIBG, P-75	75 (520)	200 (1380)
5	Boron	58 (400)	400 (2760)
6	PIBG, P-55	55 (380)	200 (1380)
7	PABG, high modulus	53 (365)	260 (1795)
8	PABG, intermed. modulus	42 (290)	750 (5170)
9	PABG, high strain	36 (250)	440 (3035)
10	PABG, high strength	34 (235)	360 (2480)
11	PIBG, P-25	20 (140)	200 (1380)
12	Kevlar-49	19 (130)	330 (2275)
13	S2-glas	13 (85)	360 (2480)
14	E-glass	10 (70)	250 (1725)

PIBG, Pitch-based graphite; PABG, pan-based graphite.

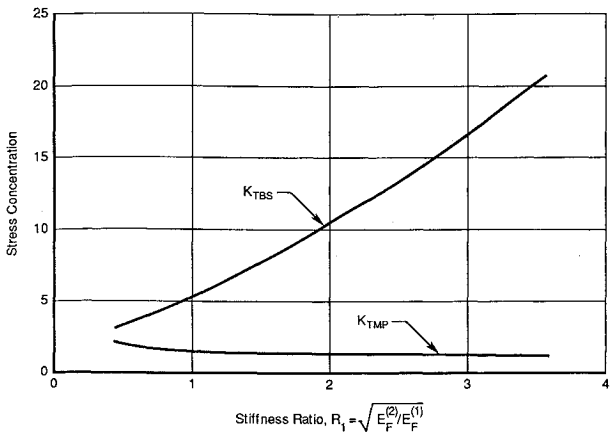

Fig. 7 Effect of stiffness on stress concentration.

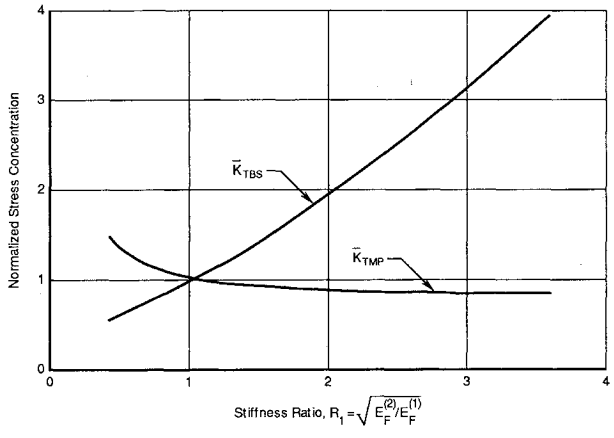

Fig. 8 Effect of stiffness on normalized stress concentration.

Table 2 Normalized failure strains, $\bar{\varepsilon}$ (%)

Main panel mat'l ID#	Buffer strip material ID#													
	1	2	3	4	5	6	7	8	9	10	11	12	13	14
1	100	113	75	101	220	112	147	458	256	235	152	256	309	226
2	85	100	67	89	196	100	131	410	230	211	138	233	283	209
3	124	145	100	133	294	150	197	619	348	320	211	357	436	323
4	93	109	75	100	220	112	148	464	261	240	158	268	327	242
5	41	48	33	44	100	51	67	212	119	110	73	123	152	113
6	80	94	65	86	195	100	132	415	234	215	143	243	299	222
7	60	71	49	65	147	76	100	315	178	163	109	184	227	169
8	19	22	15	20	46	23	31	100	57	52	35	59	73	55
9	32	38	26	35	80	41	54	174	100	92	62	105	131	98
10	36	41	28	38	86	44	58	188	108	100	68	115	142	107
11	44	56	40	53	120	61	81	263	151	140	100	170	214	161
12	26	32	24	32	70	36	47	153	88	81	58	100	126	95
13	18	23	17	22	53	27	37	117	67	62	45	76	100	76
14	23	28	20	27	65	34	45	153	86	80	57	98	129	100

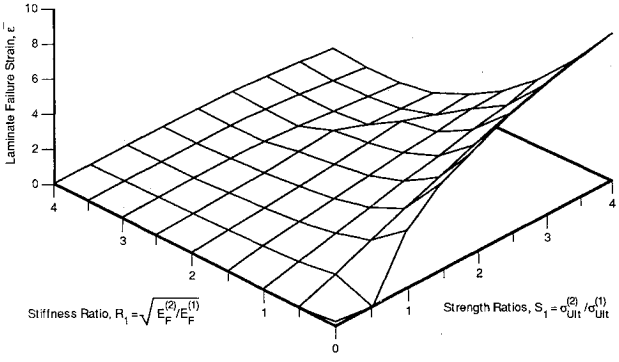

Fig. 9 Dependence of failure strain on stiffness and strength.

The stress concentrations in the critical fibers of the buffer strips and the main panel as defined in Eq. (16) are plotted in Fig. 7 for various stiffness ratios. For the case of a simple laminate without buffer strips, $R_1 = 1$, the stress concentration at the edge of the cutout is 5.25. Some interesting observations can be made by comparing the results of buffer strip laminate with a cutout to those of a simple (one material) laminate without buffer strips. Define a set of normalized stress concentrations as

$$\bar{K}_{TBS} = K_{TBS}^{(R)}/K_{TBS}(R = 1)$$
$$\bar{K}_{TMP} = K_{TMP}^{(R)}/K_{TMP}(R = 1) \tag{18}$$

These normalized stress concentrations are plotted in Fig. 8. we observe that $K_{TBS} \leq 1$ and $\bar{K}_{TMP} \geq 1$ for $R_1 \leq 1$, that is, for softer buffer strips. The benefits of having a reduced stress concentration at the cutout edge is negated by an increase in stress concentration in the main panel by using buffer strips that are too soft. This point will be further elaborated when failure strains for the laminate are considered.

Both the stiffness and the strength of the buffer strip affect the failure of the critical fiber of the laminate. Define the normalized failure strain

$$\bar{\varepsilon} = \varepsilon_{BS}/\varepsilon_{REF} \tag{19}$$

where ε_{BS} is the remote strain required to break the critical fiber of a laminate with buffer and ε_{REF} is the corresponding strain for a luminate without buffer strips. A value $\bar{\varepsilon} = 1$ indicates that there is no increase in the failure strain by using buffer strips. The normalized failure strains for various combinations of main panel and buffer strip materials are shown in Table 2. The effectiveness of buffer strips is indicated by a higher value of normalized failure strain. Buffer strips made of material 3 are not at all effective in increasing the notched strength of panels of any one of the remaining 13 materials. Even though material 3 has a high modulus, the fact that it has the lowest tensile strength makes it very ineffective. On the other hand, material 8, when used as a buffer strip, enhances the notched strength of a panel made of any one of the remaining materials. It is interesting to note that this material has a moderate stiffness but the highest tensile strength. Further, material 8 has a much higher failure strain than ma-

terial 3. Failure strain of the buffer strip material plays a dominant role in the effectiveness of the bufferstrip; however, it is not the only parameter that influences the laminate failure strain. In this context, a comparison of material 8 and 12 reveals that both materials have the same failure strain (1.78%), but material 12 is not as effective as material 8 when used as the buffer strip material. A plot of these results using the stiffness ratio R_1 and strength ratio S_1 is shown in Fig. 9. It is apparent from this graph that softer and stronger buffer strips ($R_1 < 1$ and $S_1 > 1$) are most efficient in increasing the notched strength of laminates with circular cutouts.

Appendix

The functions K_{ij} in Eq. (15) are given by

$$K_{11} = \frac{2}{\pi}\int_0^{\pi} e^{-\delta\eta_n}[\delta c(n) + \bar{\alpha}_n F_n]c(m)\,d\theta$$

$$K_{12} = -K_{13} = \frac{1}{\pi}\int_0^{\pi} F_{NW1}\left[\frac{\bar{\alpha}_n}{\delta}F_n D(\delta, \eta_n, t) - (e^{-\delta(\eta_n+t)} + pe^{-\delta|\eta_n-t|})c(n)\right]d\theta$$

$$K_{14} = -\frac{1}{\pi}\int_0^{\pi} F_N\left[\frac{\bar{\alpha}_n}{\delta}F_n D(\delta,\eta_n,t) - (e^{-\delta(\eta_n+t)} + pe^{-\delta|\eta_n-t|})c(n)\right]d\theta$$

$$K_{21} = K_{31} = \frac{2}{\pi}\int_0^{\pi} e^{-\delta\eta}c(m)c(NW1)\,d\theta$$

$$K_{22} = \frac{1}{\pi}\int_0^{\pi}\left[\frac{F_{NW1}}{\delta}D(\delta, \eta, t)c(NW1) + \frac{c^2(0)}{R_1\delta}D(\delta_n, \eta, t)\right]d\theta$$

$$K_{23} = -\frac{1}{\pi}\int_0^{\pi}\frac{F_{NW1}}{\delta}D(\delta, \eta, t)c(NW1)\,d\theta$$

$$K_{24} = -\frac{1}{\pi}\int_0^{\pi}\frac{F_N}{\delta}D(\delta, \eta, t)c(NW1)\,d\theta$$

$$K_{25} = -K_{26} = \frac{R_1}{\pi}\int_0^{\pi}\frac{F_{NW2}}{\delta}c(0)D(\delta, \eta/R_1, t)\,d\theta$$

$$K_{32} = \frac{1}{\pi}\int_0^{\pi}\frac{1}{\delta}[F_{NW1}c(NW1) + c^2(0)]\,d\theta$$

$$K_{33} = -\frac{1}{\pi}\int_0^{\pi}\frac{F_{NW1}}{\delta}c(NW1)\,d\theta$$

$$K_{34} = -\frac{1}{\pi}\int_0^{\pi}\frac{F_N}{\delta}c(NW1)\,d\theta$$

$$K_{41} = \frac{2}{\pi}\int_0^{\pi} e^{-\delta\eta}F_N c(m)\,d\theta$$

$$K_{42} = -K_{43} = \frac{1}{\pi}\int_0^{\pi}\frac{F_N F_{NW1}}{\delta}D(\delta, \eta, t)\,d\theta$$

$$K_{44} = -\frac{1}{\pi}\int_0^{\pi}\frac{F_N^2}{\delta}D(\delta, \eta, t)\,d\theta$$

$$K_{52} = -K_{62} = \frac{1}{\pi R_1^2}\int_0^{\pi}\frac{c(0)}{\delta}c(NW2)D(\delta, \eta, t/R_1)\,d\theta$$

$$K_{55} = \frac{1}{\pi R_2}\int_0^{\pi}\frac{1}{\delta}[D(\delta_2, \eta, t)c^2(0) + R_2 D(\delta, \eta, t)F_{NW2}c(NW2)]\,d\theta$$

$$K_{56} = -\frac{1}{\pi}\int_0^{\pi}\frac{1}{\delta}D(\delta, \eta, t)F_{NW2}c(NW2)\,d\theta$$

$$K_{65} = \frac{1}{\pi}\int_0^{\pi}\frac{1}{\delta}[D(\delta, \eta, t)F_{NW2}c(NW2) + D(\delta_2, \eta, t)c^2(0)]\,d\theta$$

$$K_{66} = -\frac{1}{\pi}\int_0^{\pi}\frac{1}{\delta}D(\delta, \eta, t)F_{NW2}c(NW2)\,d\theta$$

$$K_{15} = K_{16} = K_{35} = K_{36} = K_{45} = K_{46} = K_{53} = K_{54} = K_{61} = K_{63} = K_{64} = 0$$

where

$$\bar{\alpha}_n = \frac{\alpha_n}{\sqrt{1 - \alpha_n H_o}}$$

$$p = -1 \text{ for } t < \eta_n \quad \text{and} \quad p = 1 \text{ for } t \leq \eta_n$$

$$R_i = \frac{\psi^{(i+1)}}{\psi^{(i)}}, \quad \delta_i = \delta/R_i$$

The coefficients K_{ij} are written assuming that all the three regions and the interfaces between adjoining regions have the same shear stiffness.

References

[1]Cherry, F. D., "Elimination of Fastener Hole Stress Concentrations Through the Use of Softening Strips," *Proceedings of the Conference on Fibrous Composites in Flight Vehicle Design*, AFFDL-TR-72-130, 1972.

[2]Verette, R. M., and Labor, J. D., "Structural Criteria for Advanced Composites," AFFDL-TR-76-142, 1976.

[3]Sun, C. T., and Voit, P. M., "Improvement of the First-Ply-Failure Strength in Laminates by Using Softening Strips," *Composites Technology Review*, Vol. 3, 1981, pp. 109–113.

[4]Sun, C. T., and Luo, J., "Failure Loads for Notched Graphite/Epoxy Laminates with a Softening Strip," *Composites Science and Technology*, Vol. 22, 1985, pp. 121–33.

[5]Poe, C. C., Jr., and Kennedy, J. M., "An Assessment of Buffer Strips for Improving Damage Tolerance of Composite Laminates," *Journal of Composite Materials Supplement*, Vol. 14, 1980, pp. 55–70.

[6]Dharani, L. R., and Goree, J. G., "Analysis of a Unidirectional, Symmetric Buffer Strip Laminate with Damage," *Engineering Fracture Mechanics*, Vol. 20, 1984, pp. 801–811.

[7]Dharani, L. R., and Seaton, C. P., "Analysis of a Buffer Strip Laminate with Fiber and Matrix Damage and Interlaminar Debonding," *Composite Structures*, Vol. 7, 1987, pp. 139–158.

[8]Dharani, L R., "An Assessment of Buffer Strips for Reduction of Stress Concentration at Cutouts in Composite Laminates," *Composites Science and Technology*, Vol. 30, 1987, pp. 221–231.

[9]Hedgepeth, J. M., "Stress Concentrations in Filamentary Structures," NASA TN D-882, 1961.

[10]Hedgepeth, J. M., and VanDyke, P., "Local Stress Concentrations in Filamentary Composite Materials," *Journal of Composite Materials*, Vol. 1, 1967, pp. 291–309.

[11]Goree, J. G., and Gross, R. S., "Analysis of a Unidirectional Composite Containing Broken Fibers and Matrix Damage," *Engineering Fracture Mechanics*, Vol. 13, 1979, pp. 563–578.

[12]Jones, W. F., "Unidirectional Composite Laminates with Circular and Rectangular Cutouts," Master of Science Thesis, Clemson University, Clemson, SC, 1981.

[13]Dharani, L. R., Jones, W. F., and Goree, J. G., "Mathematical Modeling of Damage in Unidirectional Composites," *Engineering Fracture Mechanics*, Vol. 17, 1983, pp. 555–573.